Article | Received 28 April 2025; Accepted 26 June 2025; Published 21 July 2025
https://doi.org/10.55092/sc20250018

Adaptability analysis of autonomous vehicles on small-radius circular curves based on co-simulation

Zhiqing Zhang[1], Xiaozheng Yu[1], Leipeng Zhu[1] and Min Wang[2,*]

[1] Beijing Key Laboratory of Traffic Engineering, Beijing University of Technology, Beijing, China
[2] Department of Management Science and Statistics, The University of Texas, San Antonio, USA

* Correspondence author; E-mail: min.wang3@utsa.edu.

Highlights:

- A co-simulation framework evaluates AVs adaptability on small-radius curves with radii from 60–700 m.
- When the critical adhesion coefficient μ exceeds 0.2 at R ≤ 200 m, ride comfort degrades to 'moderately uncomfortable' level.
- Speed-radius coupling shows 70–100 km/h improves comfort to Level 1–2 at typical minimum radii.
- Current road standards fail to meet AVs comfort needs at minimum radii.

Abstract: With the rapid development of autonomous driving technology, the incompatibility between traditional road infrastructure and autonomous vehicles (AVs) has become increasingly prominent. This study focuses on small-radius circular curves as a typical challenging alignment feature and systematically analyzes the dynamic response characteristics of AVs under varying speeds and curve radii, ranging from the minimum limit radius to the general minimum radius, A high-fidelity Prescan-Carsim-Simulink co-simulation platform is employed to evaluate the intrinsic relationship between vehicle driving safety, ride comfort, and curve radius. The results indicate that under low-speed conditions (40–60 km/h), when the curve radius approaches the minimum limit, the peak lateral acceleration (0.2–0.4 g) and critical adhesion coefficient (0.15–0.22) substantially reduce the vehicle's safety margin and degrade occupant comfort to levels 3 (moderately uncomfortable). In contrast, at higher speed (70–100 km/h) combined with larger radii (general minimum), the dynamic response become more stable, improving comfort to levels 1–2 (comfortable to moderately comfortable). This study provides a theoretical basis for the design of road alignment in autonomous driving environments and offers practical recommendations for adapting existing roads and optimizing autonomous driving systems for improved safety and comfort.

Keywords: autonomous vehicles; small-radius circular curves; adaptability; co-simulation

1. Introduction

Autonomous vehicles (AVs) are expected to reduce approximately 90% of traffic accidents caused by human error [1]. Nevertheless, current road alignment design standards are still primarily based on the needs for conventional human-operated vehicles and do not sufficiently account for the unique operational characteristics of autonomous driving systems [2]. Under challenging geometric configurations, particularly small-radius horizontal curves, AVs often struggle critical deficiencies in lateral stability control, path-tracking precision, and ride comfort metrics [4]. To address these challenges, multi-software co-simulation and digital twin technologies have emerged as predominant methodologies in the testing and evaluation of AVs [5]. By integrating Prescan (road environment modeling), CarSim (vehicle dynamics simulation), and Simulink (control algorithm design), researchers can systematically evaluate AVs' dynamic responses under diverse road alignment conditions [6].

For instance, Ye *et al.* [7] examined the effects of road design parameters, such as stopping sight distance and vertical curve length on occupant comfort, and revealed that AV systems tend to have more lenient requirements for road geometry compared to conventional vehicles. In contrast, Lengyel [8] identified significant incompatibility between intelligent vehicles equipped with adaptive cruise control and lane-keeping systems with existing road infrastructure, although the study did not explore the specific effects of small-radius curve impacts. Chang *et al.* [9] conducted on-road driving tests to analyze factors affecting the safety of Level 2 autonomous vehicles when navigating curves, concluding that the smaller the curve radius and the higher the vehicle speed, the greater the ADAS disengagement rate. Similarly. Wang *et al.* [10] quantified the differences in stopping sight distance (SSD) requirements across automation levels, revealing that Level 1–3 AVs demand higher alignment standards than human-driven vehicles, whereas Level 4–5 AVs exhibit more flexible geometric adaptability. Alfredo Garcia *et al.* [11] analyzed horizontal alignment adaptability through using AV disengagement as thresholds, identifying a strong correlation between curve radius and operating speed, while also noting inferior performance of low-level AVs on small-radius curves. Xia [12], using a Carsim-Simulink joint simulation platform and real-vehicle validation, found that perception limitations due to the blind area of the field of view, could substantially reduce AV driving safety when navigating small-radius curves, thus exposing technical shortcomings under current system under the complex linear conditions.

Notably, these studies primarily compare human-driven and AV performance (e.g., sight distance, disengagement rates) but overlook intrinsic vehicle dynamics-particularly lateral acceleration and adhesion coefficients, which critically influence safety and comfort.

Zhou [13] developed a Prescan-CarSim-Simulink integrated platform to investigate the formulation of hazardous scenario for adaptive cruise-controlled vehicles across different alignments. Ning *et al.* [14] proposed an AV accident prediction model for high-risk road segments through using Chang'an University's IoV and AV test platform. identifying horizontal curve deflection angle, lateral force coefficient, and longitudinal slope as critical safety factors. Wang *et al.* [15] established a PreScan-Simulink hybrid simulation framework to quantify trajectory deviation patterns relative to geometric parameters, demonstrating through empirical data that a combination of inner lanes, downhill sections, and left-turn curves could significantly exacerbate trajectory anomalies.

Of particular note is that most existing research has centered on large-radius horizontal curves, with limited investigation into adverse geometric conditions, such as small-radius circular curves. In

particular, systematic analyses quantifying ride comfort under such conditions remain notably absent. To address this gap, the present study focuses specifically on small-radius circular curve segments by establishing a high-fidelity Prescan-CarSim-Simulink co-simulation platform. The research systematically evaluates dynamic response characteristics of AVs under these challenging geometric conditions, with a particular emphasis on elucidating the mechanistic impacts of small-radius curves on both driving safety and occupant comfort. These findings are expected to provide a theoretical foundation for optimizing road alignment and enhancing autonomous driving systems.

The structure of this paper is organized as follows. Section 2 describes the co-simulation framework and control algorithm design. Section 3 introduces the evaluation metrics and experimental setup for circular curve adaptability. Section 4 presents the simulation results and analysis of AVs safety and comfort. Section 5 concludes the study and discusses future work.

2. Implementation of a co-simulation framework for AVs testing

This platform employs a decoupled lateral-longitudinal control strategy, utilizing a discrete Linear Quadratic Regulator (LQR) algorithm for lateral trajectory tracking while integrating Proportional-Integral-Derivative (PID) control for longitudinal speed regulation, thereby establishing a comprehensive closed-loop autonomous driving control system.

2.1. Control algorithm and simulation architecturef design

2.1.1. Discrete LQR-based lateral control model for AVs

(a) Vehicle coordinate system selection

This study employs the Frenet Coordinates to decouple vehicle kinematics, decomposing vehicle motion into longitudinal motion (along the trajectory) and lateral motion (perpendicular to the trajectory). A key advantage of this approach lies in its parametric curve representation, which enables the decoupling of vehicle dynamics and significantly simplifies the computational framework for control algorithms, such as LQR.

(b) Vehicle dynamic model formulation

This study establishes a two-degree-of-freedom (2-DOF) vehicle dynamics model based on the following two assumptions: (1) small front-wheel steering angle (δ_f) and (2) constant longitudinal velocity (v_x). The model aligns with the decoupled control paradigm for lateral and longitudinal motion, while incorporating nonlinear tire characteristics to significantly improve its fidelity to real-world vehicle behavior. The schematic representation of the model is illustrated in Figure 1.

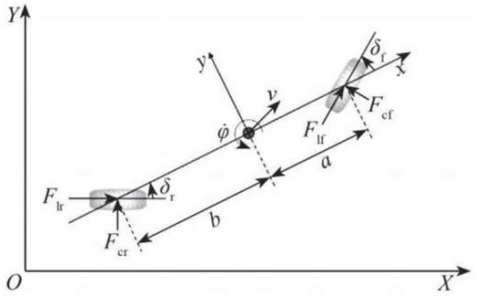

Figure 1. Vehicle dynamics model.

(c) Discrete LQR control strategy

As a cornerstone of modern optimal control theory, LQR leverages a full-state linear feedback mechanism to construct closed-loop optimal control systems. Compared to conventional control strategies, LQR demonstrates superior tracking precision and robustness. In this study, the cost function of LQR is formalized as Equation (1).

$$J = e_{rr}^T Q e_{rr} + u^T R u \tag{1}$$

where e_{rr} represents the lateral deviation between the vehicle's true position and its projected reference position on the trajectory, Q and R represent the state and input weighting matrices, respectively. The control problem is subsequently transformed into a constrained optimization framework under linear system dynamics, enabling real-time implementation through discrete-time formulations.

The feedforward control input integrates three key components: vehicle parameters (e.g., mass, inertia), the LQR-generated gain matrix K, and the reference curvature k derived from the error calculation module. This integration process enables systematic compensation for trajectory tracking deviations through proactive actuation commands given by

$$f_c = k[a+b-bK_x - \frac{mv_x^2}{a+b}(\frac{b}{C_{\alpha f}} + \frac{a}{C_{\alpha r}}K_x - \frac{a}{C_{\alpha r}})] \tag{2}$$

$$\delta = -Ke_{rr} + f_c \tag{3}$$

where K represents the state feedback gain matrix generated by the LQR controller, k denotes the reference curvature derived from the trajectory planning module, and v_x is the longitudinal velocity of the vehicle (assumed constant). The parameters a and b indicate the distances from the vehicle's center of mass to the front axle and rear axle, respectively, while $C_{\alpha f}$ and $C_{\alpha r}$ represent the cornering stiffness of the front and rear tires, respectively.

2.1.2. Discrete PID-based longitudinal control model for AVs

This study employs a systematic calibration methodology, wherein incremental accelerator pedal inputs are applied to characterize the corresponding velocity (v) and acceleration (a) profiles. The resultant v-a characteristic map is subsequently generated through data integration. The comprehensive workflow for longitudinal control implementation is illustrated in Figure 2.

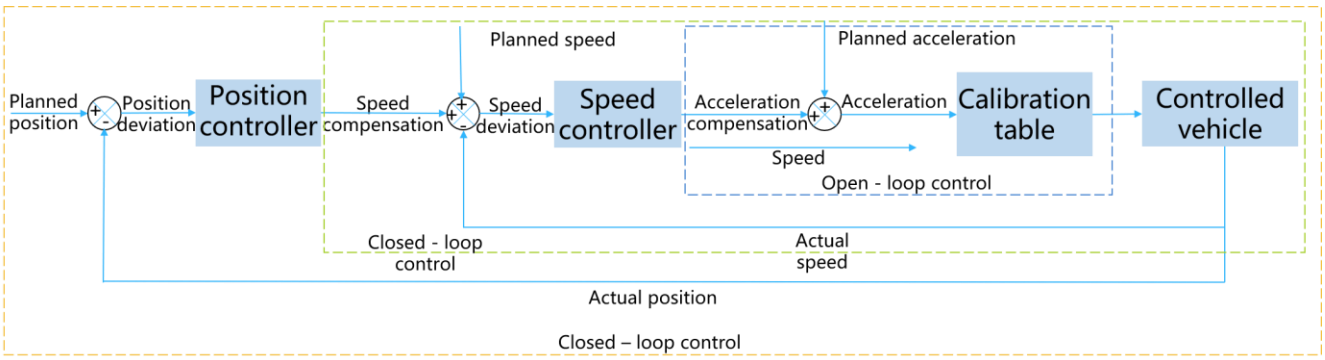

Figure 2. Longitudinal control flow.

The longitudinal control system employs a cascaded PID control architecture that comprises two hierarchical control loops. The outer-loop position PID controller regulates the longitudinal tracking error (e_s) between the desired and actual vehicle positions, while the inner-loop velocity PID controller processes the position controller's output reference by integrating real-time velocity feedback with trajectory planning constraints to generate actuation commands. The system interfaces with the vehicle's drivetrain through a pre-calibrated throttle/brake look-up table that translates control signals into actuator outputs, thereby achieving precise longitudinal motion control. The mathematical formulation of this control strategy that explicitly captures the coupled dynamics of both control loops is presented in Equation (4),

$$u(t) = K_p e(t) + K_i T \sum_{j=0}^{t} e(j) + K_d \frac{e(t) - e(t-1)}{T} \tag{4}$$

where the PID controller gains K_p, K_i, and K_d represent the proportional, integral, and derivative coefficients, respectively. The control output $u(t)$ provides normalized actuation commands ranging from −1 (full braking) to +1 (full throttle), t represents the sampling index, T denotes the sampling interval, e(t) corresponds to the current error term, and e(t-1) signifies the preceding error term from the last sampling instant.

2.1.3. Prescan-Carsim-Simulink co-simulation test platform

After loading the PreScan scenario in MATLAB/Simulink, the 'Audi A8 Sedan' is selected as the ego vehicle, and control algorithm modules are integrated. The operational interface comprises three core components: the PreScan environment module, the control module, and the CarSim vehicle dynamics module, as illustrated in Figure 3.

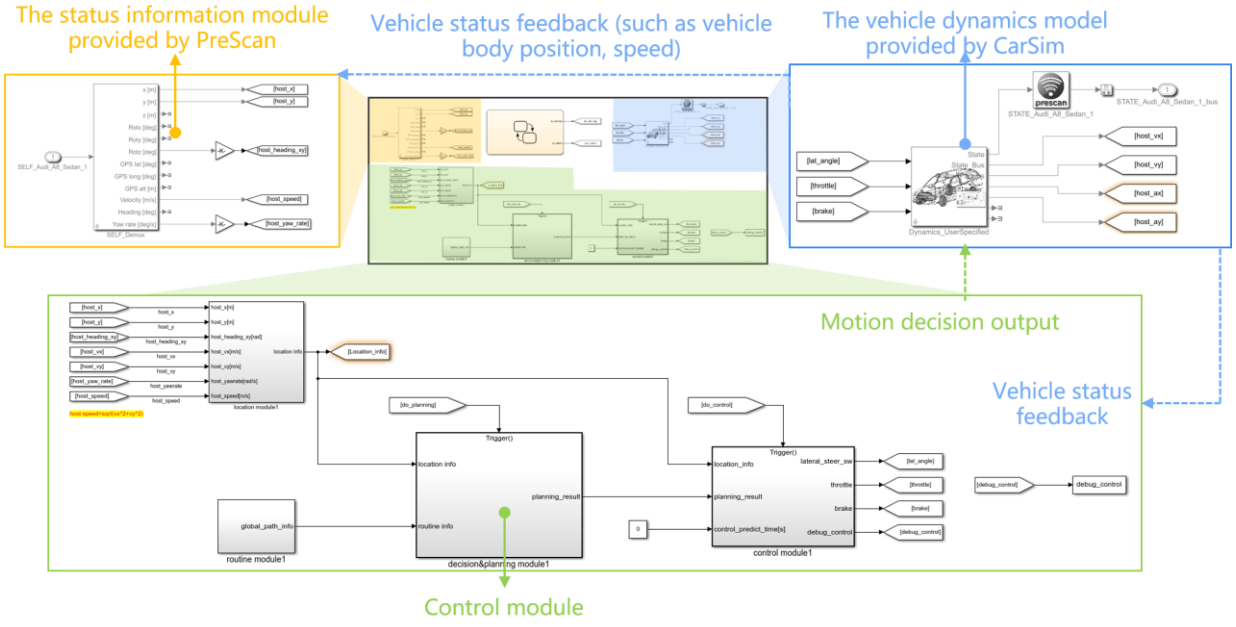

Figure 3. Connection diagram of each control module.

2.2. Test scenario construction

2.2.1. Parametric road alignment modeling based on Prescan

Based on the geometric characteristics of road alignments, this study categorizes roads into three fundamental elements: tangent segments (straight sections), transition curves (spiral sections), and circular curves, which are systematically combined to construct comprehensive test scenarios. The parametric modeling methodology is implemented as follows:

(a) The Tangent segments were constructed using the Prescan "StraightRoad" model, with their lengths uniformly configured to 400 meters through the "Length" parameter to serve as speed stabilization zones prior to curve entry, thereby ensuring consistent initial dynamic conditions across all test scenarios.

(b) The transition curves were modeled using the "Spiral/Clothoid Road" module, with key parameters including the initial radius ("Rstart"), terminal radius ("Rend"), curve length ("ΔL" set to 250 m in this study), deflection angle ("ΔAngle"), and clothoid parameter ("Curve"). These parameters were optimized to ensure continuous and smooth curvature transitions throughout the spiral section.

(c) The circular curves were modeled using the "Bend Road" module, with geometric configurations adjusted through the radius ("Radius") and central angle ("Angle") parameters. These parameter settings were established with reference to the China's "Design Specification for Highway Alignment JTG D20-2017" [16] standards, while incorporating appropriate modifications to address the specific requirements of AVs.

2.2.2. Vehicle dynamics modeling based on CarSim

To achieve high-precision vehicle dynamics simulation, the six-degree-of-freedom parametric "Vehicle Dynamics" model in CarSim was employed to replace the basic dynamics model in Prescan. The Audi A8 Sedan was selected as the test vehicle for this study.

Within the main control panel, the "CarSim Vehicle Dynamics" model allows for configuration of the simulation working directory, sampling frequency, parameter output frequency, and input/output parameters. For this study, both the simulation sampling frequency and data output frequency were set to 1000 Hz to adequately capture the transient characteristics of vehicle dynamics. The input and output parameters were retained at their default values (23 input parameters and 35 output parameters) without additional modifications.

2.3. Platform verification criteria

To ensure the validity of subsequent research on the applicability of China's highway alignment indicators, the stability and reliability of the co-simulation platform must be verified before conducting simulation experiments. This study adopts a combined lane-changing and braking scenario [17] as the test condition, with verification criteria including: centimeter-level trajectory tracking accuracy (< 0.1 m deviation between actual and desired paths), stable speed control with acceleration fluctuations limited to 0.2 m/s² (excluding initial acceleration and final deceleration phases), and constrained lateral acceleration variations (< 0.2 g) to prevent driving discomfort. These verification results will be

presented in Section 3.1, providing a reliable data foundation for subsequent investigations of autonomous vehicle adaptation on circular curve segments.

3. Circular curve adaptability evaluation framework

3.1. Evaluation indexes of the lateral and longitudinal stability of vehicles

3.1.1. Speed

Speed serves as a fundamental operational parameter in vehicular transportation, manifesting throughout all phases of road design and operation. Current regulations specify maximum permissible speeds of 120 km/h on operational roadways, while Grade II and higher-class highways mandate minimum speeds of 40 km/h. Given the operational design domain constraints of AVs, their operational speeds typically exceed 40 km/h. Furthermore, high-grade highways adhere to more stringent geometric design standards with superior roadside conditions. Research indicates that when vehicle speeds exceed 100 km/h, driving risks are seldom attributable to the autonomous system itself [18]. Consequently, this study establishes the operational speed range as: 40 km/h $\leq V_{de} <$ 100 km/h.

3.1.2. Lateral acceleration (A_y)

Lateral acceleration, as a fundamental evaluation parameter for both vehicle safety and occupant comfort, directly influences dynamic vehicle responses through its temporal distribution. From a safety perspective, when the magnitude of lateral acceleration exceeds critical thresholds, the frictional equilibrium at the tire-road interface becomes compromised, subsequently inducing skid risks. Excessive lateral acceleration increases drivers' neuromuscular load (causing tension and fatigue) and amplifies passengers' perception of lateral motion, reducing comfort ratings.

This study establishes lateral acceleration as a key control variable for evaluating cornering stability. Empirical studies demonstrate that safety boundaries vary across vehicle types: standard passenger vehicles require limitation below 0.4 g [19]. Beyond this threshold, tire cornering stiffness exhibits pronounced nonlinear characteristics, impairing stable curvature tracking and introducing instability risks. Given this study's focus on light passenger vehicles, the safety-critical threshold is set at $A_y \leq 0.4$ g.

From a comfort standpoint, lateral acceleration magnitude directly determines passenger comfort levels. Following German research findings [20,21], lateral acceleration values are classified into four comfort grades, as detailed in Table 1.

Table 1. The absolute value of lateral acceleration corresponds to the level of ride comfort.

Comfort Level	Level 1	Level 2	Level 3	Level 4
Passenger perception	Comfortable	moderately comfortable	moderately uncomfortable	uncomfortable
A_y (m/s^2)	[0, 1.8]	[1.8, 3.6]	[3.6, 5]	[5, +∞]

Comfort indicates that occupants are completely unaware of road alignment variations, exhibit no physiological discomfort responses, and the vehicle maintains stable operational conditions. Moderately comfortable implies occupants begin to perceive road alignment characteristics with slight discomfort, while vehicle dynamics remain fundamentally stable. Moderately uncomfortable denotes occupants

persistently experience alignment-induced effects with significantly reduced comfort levels, accompanied by occasional unstable vehicle oscillations. Uncomfortable refers to situations exceeding occupants' physiological tolerance limits, with the system demonstrating sustained stability failures.

The adhesion characteristics at the tire-road interface constitute the fundamental constraint for vehicle dynamic stability. When lateral forces act upon tires, the road surface must generate sufficient normal adhesion effects to mitigate potential skid conditions. This study defines the adhesion coefficient φ as the ratio of lateral force to vertical load for each passenger vehicle wheel, with the critical adhesion coefficient μ established as the peak absolute value of φ, as formulated in Equation (5):

$$\varphi = \frac{F_{yi}}{F_{zi}} \tag{5}$$

where φ denotes the adhesion coefficient; F_{yi} represents the tire lateral force (N); F_{zi} indicates the tire vertical force; i (i = 1, 2, 3, 4) corresponds to the front-left, front-right, rear-left, and rear-right wheels, respectively; $\mu = \max\varphi$ is defined as the critical adhesion coefficient.

A higher $\Delta\mu$ value indicates greater vehicle safety margin during operation. Conversely, when Δμ approaches zero, it signifies that the available road adhesion capacity is nearly exhausted by the applied lateral tire forces, placing the vehicle in imminent skid risk. The condition $\Delta\mu \leq 0$ indicates that the lateral tire forces have exceeded the maximum available road adhesion, resulting in high skid probability. Therefore, to ensure safe vehicle operation, the constraint in Equation (6) must be satisfied

$$\psi > \mu \tag{6}$$

In vehicle dynamics research, the safety threshold for lateral acceleration is typically set at 0.4 g, which is intrinsically linked to the road surface's critical adhesion coefficient in Table 2 and proven effective in preventing lateral slip. As shown in Table 3, the critical adhesion coefficient μ serves as a key indicator for evaluating occupant comfort on curved segments. Consequently, practical applications require comprehensive consideration of the interrelationship between adhesion coefficient and lateral acceleration, with μ-A_y coupling analysis ensuring both driving safety and ride comfort.

Table 2. Adhesion coefficient of pavement under different speed in dry environment.

V_{de} ((km/h)	40	50	60	70	80	90	100
Road surface adhesion coefficient ψ	0.72	0.66	0.60	0.55	0.49	0.43	0.38

Table 3. The critical adhesion coefficient corresponds to the level of ride comfort.

Comfort Level	Level 1	Level 2	Level 3	Level 4
Passenger perception	comfortable	moderately comfortable	moderately uncomfortable	uncomfortable
Critical adhesion coefficient μ	[0, 0.15]	[0.15, 0.2]	[0.2, 0.35]	[0.35, +∞]

3.2. Study on circular curve radius selection

To evaluate AV safety and comfort on small-radius curves, simulations covered speed-radius combinations from absolute to typical minimum radius. With reference to the lateral friction coefficient specifications in the Technical Standard of Highway Engineering [22] and accounting for practical requirements, interpolation methods were employed to calculate the absolute and typical minimum radii for circular curves at different speeds. For the absolute minimum radius calculations, a maximum superelevation rate of 8% (i_H = 8%) was adopted with lateral friction coefficients ranging from 0.10 to 0.17, while the typical minimum radius calculations used a 6% superelevation rate (i_H = 6%) with lateral friction coefficients between 0.05 and 0.06.

The research focused on analyzing the minimum comfort radius adaptable by autonomous driving systems, while examining the operational range from absolute to typical minimum radii across varying speeds, with the objective of determining the minimum safe radius for autonomous vehicle operation. By establishing speed-radius correlation matrices (Table 4), this study provides both theoretical foundations for road alignment design and quantitative references for evaluating the compatibility of existing road infrastructure.

Table 4. R-value space.

V_{de} (km/h)	40	50	60	70	80	90	100
R **(m)**	[60, 100]	[100, 150]	[125, 200]	[200,300]	[250, 400]	[325, 550]	[400, 700]
Step (m)				25			

3.3. Simulation experiment design

This section designs testing scenarios for evaluating AVs motion/dynamic response parameters on circular curves, following the scenario definition framework of Germany's PEGASUS project through a hierarchical structure of functional-logical-concrete scenarios. The experiments aim to investigate the influence of road alignment conditions on AVs operational stability, ride comfort, and safety performance.

3.3.1. Functional scenario definition

Functional scenarios form the foundational framework of the experiment. The baseline scenario in this study is defined as an autonomous vehicle maintaining steady-state operation along predefined road alignments. To ensure environmental singularity, AVs operates exclusively within a single-lane configuration without lane-changing maneuvers throughout the test. For a precise evaluation of road geometric parameters' isolated effects on vehicle dynamic responses, the experimental design enforces strict coincidence between the desired trajectory and lane centerline, thereby eliminating interference from other traffic elements.

3.3.2. Logical scenario design

Logical scenarios represent the concrete implementation of functional scenarios. The logical scenario design in this study comprises the following components:

(a) Vehicle parameters

The Audi A8 Sedan serves as the test vehicle, with its dynamic parameters constituting the baseline model. Since the experiment does not involve the path decision-making functionality of the autonomous system, the vehicle is configured to follow the lane centerline by default to achieve optimal safety trajectory.

(b) Road alignment design

The geometric model consists of tangent segments, circular curves, and transition curves. To focus on the relationship between alignment parameters and vehicle mechanical responses, the experiment maintains fixed lengths for each geometric element while setting key design indices according to current technical standards. The lane width is held constant at 3.75 m with a 2% cross slope, employing an i_H transition method that rotates about the lane centerline to linearly transition from cross slope to superelevation (i_H). The road surface friction coefficient is set to 0.9 (dry conditions). Given the negligible impact of dual-lane symmetry on experimental outcomes, left-turning curves are uniformly adopted.

(1) Tangent segment

A 400-meter straight section is established as the speed stabilization zone, allowing vehicles to complete initial dynamic adjustments before entering curves. This length is determined through comprehensive consideration of the 20 V principle (20 times the design speed distance) and experimental data stability requirements, effectively isolating acceleration phase fluctuations from curve segment test data.

(2) Transition curve

Aligned with PreScan modeling specifications, transition curve parameters include initial/final radii, length, and azimuth angle. The minimum transition curve length is set at 100 m for a design speed of 120 km/h. To enhance lateral force gradient smoothness, the experiment extends transition curves to 250 m, ensuring curvature variation rates meet AVs comfort control criteria.

(3) Circular curve

The circular curve parameter system comprises arc length, radius, deflection angle, and superelevation values at endpoints. Following the 3-second travel time criterion, all speed conditions except the 40 km/h case (using 250 m curves) employ 500 m arc lengths, achieving a 2:1 circular-to-transition ratio. This larger ratio facilitates comprehensive observation of AVs dynamic characteristics under constant curvature conditions. The testing prioritizes radii ranging from absolute minimum to typical minimum values, with particular focus on high-risk small-radius scenarios.

3.3.3. Concrete scenario design

The fundamental test scenarios are constructed based on a “tangent-transition curve-circular curve-transition curve-tangent” sequence configuration, with focused analysis on the influence of radius (R) variations on vehicle dynamics. Specific scenarios include: circular curve segments with radii (R) selected from the range specified in Table 4 and arc lengths (Lc) fixed at 500 m, combined with tangent segments (L = 400 m) and transition curves (Ls = 250 m) to form basic curve scenarios following the “tangent-transition curve-circular curve-transition curve-tangent” alignment pattern. Given the primary focus on motion/dynamic response characteristics within curve segments, the target output parameters are selected as: μ (adhesion coefficient) and Ay (lateral acceleration).

4. Circular curve adaptability evaluation framework

4.1. Verification of co-simulation testing platform

The simulation results (Figure 4) demonstrate close alignment between the vehicle's actual trajectory and the desired trajectory, with centimeter-level deviations, indicating high control accuracy of the algorithm. Analysis of throttle and brake pedal control reveals that, apart from speed fluctuations during initial acceleration and final deceleration phases, the vehicle maintains stable and continuous speed variations over time, ultimately stabilizing at 0 m/s (Figure 5). Concurrently, lateral acceleration variations remain smooth with minimal oscillations, consistently confined within the (−0.2 to 0.2 m/s²) error range (Figure 6), ensuring driver comfort. These results validate the effectiveness of the developed virtual testing platform for autonomous driving function simulation.

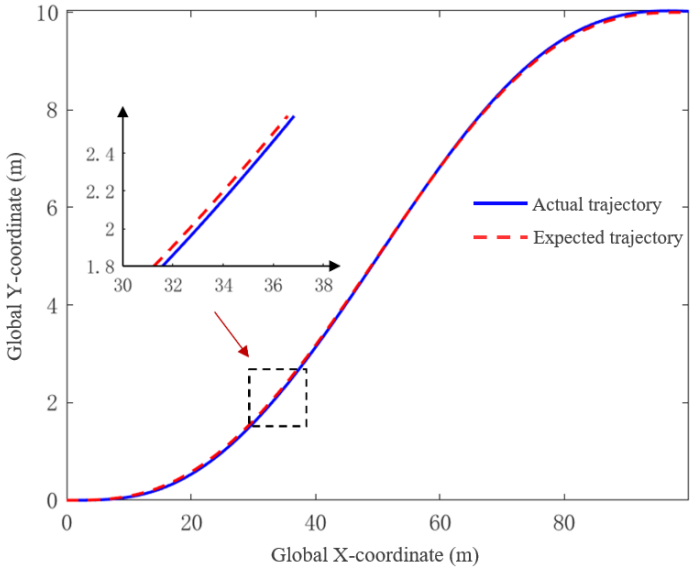

Figure 4. Actual trajectory and expected trajectory.

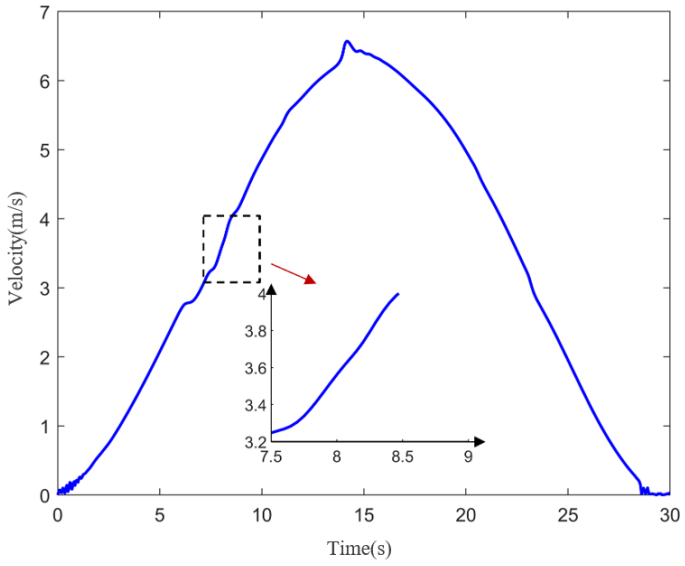

Figure 5. Velocity variation.

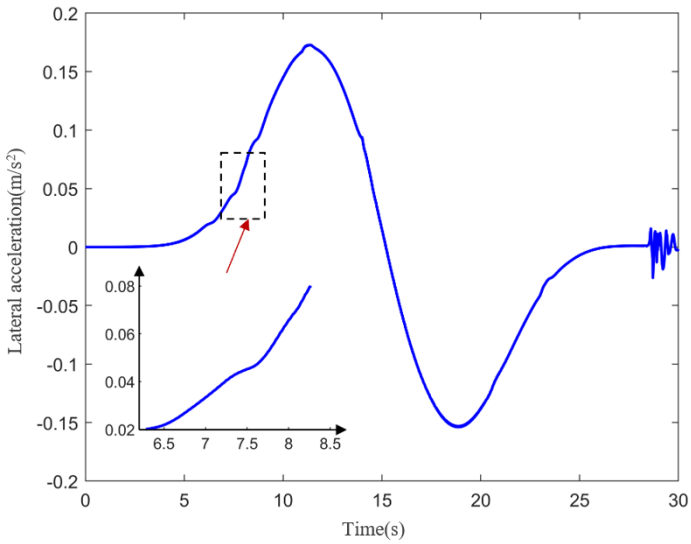

Figure 6. Lateral acceleration variation.

4.2. Adaptability analysis of circular curves

4.2.1. Motion/dynamic response parameter analysis

Figures 7–8 present the variation trends of μ (adhesion coefficient) and A_y (lateral acceleration) along the travel distance (S_{dri}) under basic curve scenarios (tangent-transition curve-circular curve-transition curve-tangent) with design speeds of 40-100 km/h and corresponding radius (R) ranges. The red dashed line marking comfort threshold, background colors denote comfort level ranges. For the 40 km/h condition, the total S_{dri} measures 1550 m (400 × 2 + 250 + 250 × 2), while other speeds feature 1800 m (400 × 2 + 250 + 250 × 2) configurations.

All response parameters oscillate along S_{dri}, peaking in circular curves, decreasing in transition curves, and stabilizing in tangent segments. The oscillation frequency exhibits an inverse relationship with amplitude.

In tangent segments, the lateral control system (LQR module) remains inactive, allowing the longitudinal controller (PID module) to maintain stable operation. Conversely, circular curves require continuous curvature input to both lateral and longitudinal controllers for trajectory correction, simulating human steering behavior.

For μ (Figure 7), values remain zero in tangent segments, rapidly increase upon entering the initial transition curve, oscillate around stable values in circular curves, then gradually decrease through the final transition curve before returning to zero in the ending tangent segment, showing symmetrical distribution. The μ values decrease with increasing R in curve segments, consistent with theoretical expectations.

Regarding A_y (Figure 8), its variation patterns and radius-dependence mirror those of μ. Equation (5) reveals that μ variations in transition curves primarily stem from vertical load redistribution between inner and outer wheels.

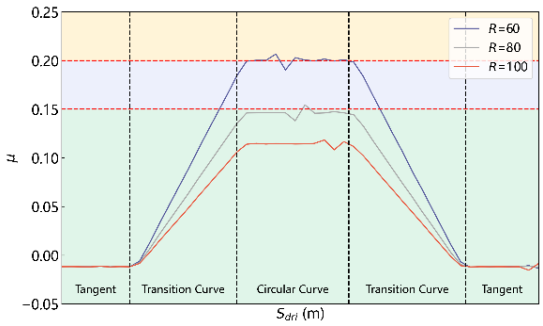

(a) V_{de} = 40 km/h

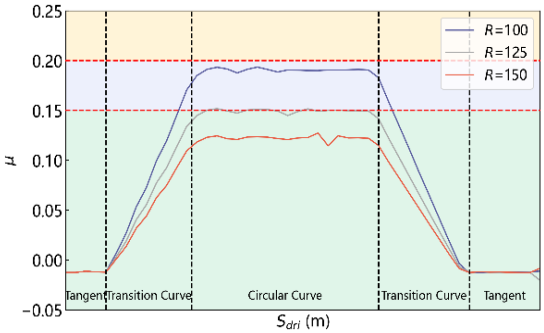

(b) V_{de} = 50 km/h

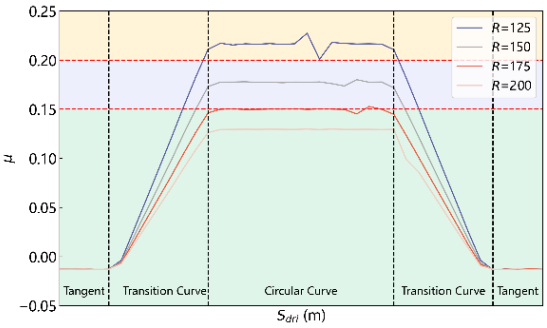

(c) V_{de} = 60 km/h

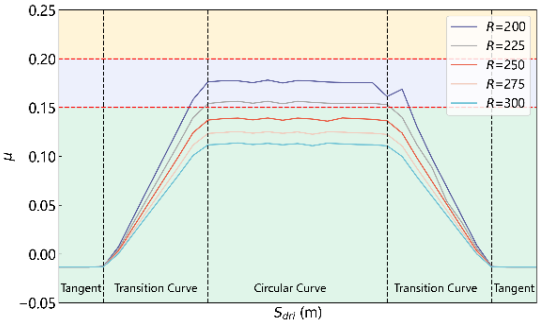

(d) V_{de} = 70 km/h

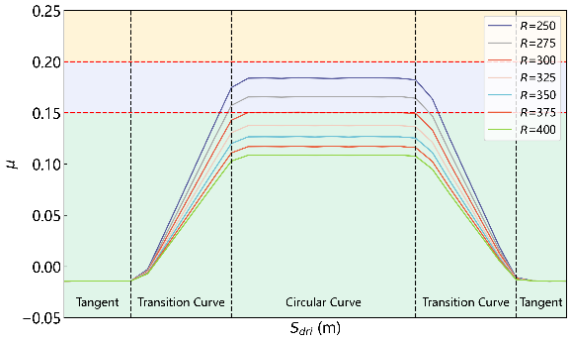

(e) V_{de} = 80 km/h

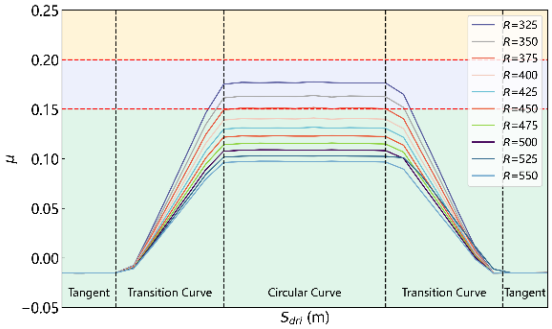

(f) V_{de} = 90 km/h

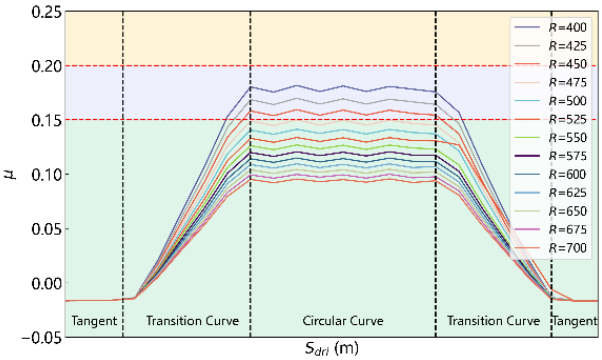

(g) V_{de} = 100 km/h

Figure 7. In the basic curve scenario, AVs μ varies with S_{dri}.

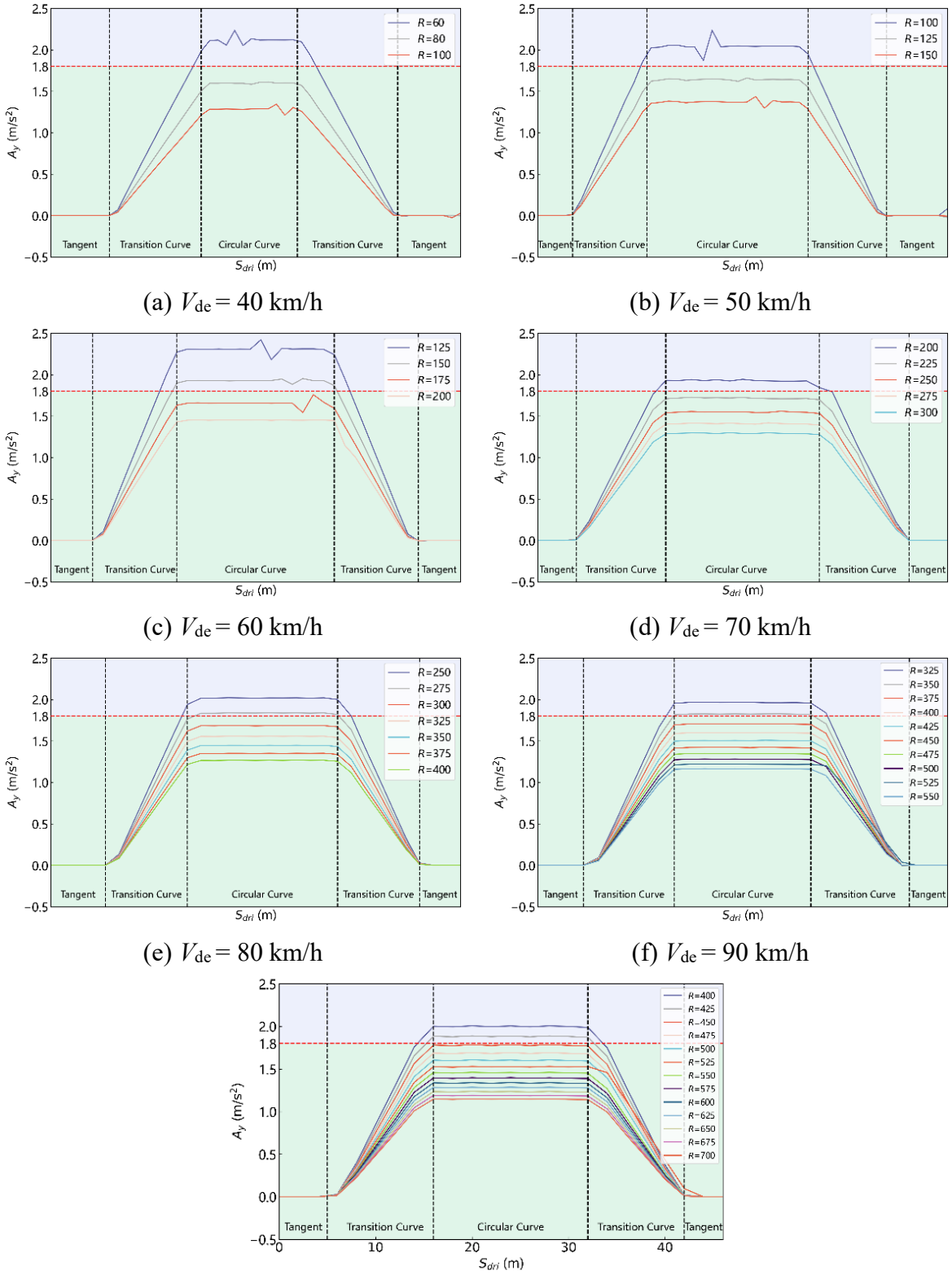

(a) V_{de} = 40 km/h (b) V_{de} = 50 km/h

(c) V_{de} = 60 km/h (d) V_{de} = 70 km/h

(e) V_{de} = 80 km/h (f) V_{de} = 90 km/h

(g) V_{de} = 100 km/h

Figure 8. In the basic curve scenario, AVs A_y varies with S_{dri}.

4.2.2. Safety and comfort-oriented circular curve adaptability analysis

Combining simulation results with the safety and comfort thresholds established in Section 2.1, this study evaluates AVs adaptability through two critical dimensions of small-radius curves.

(a) AVs safety

Analysis using dry pavement adhesion coefficients and the lateral acceleration threshold ($A_y \leq 0.4$ g) confirms (Figures 7–8, Table 5) that no scenario exceeds 0.4 g lateral acceleration, with critical μ values consistently below maximum pavement adhesion, indicating no skid risk. This conclusion is further validated by lane-keeping performance in simulation animations. Notably, μ_{max} exceeds 0.20 when speeds range 40–60 km/h with radii approaching absolute minimum values (R = 60–200 m), significantly reducing adhesion margin despite remaining within safety limits.

(b) AVs ride comfort

It is critical to note that although the 0.4 g lateral acceleration threshold meets safety requirements for conventional vehicles (as stated in Section 3.1.2), AVs require a stricter comfort limit of 0.2 g due to passengers' heightened sensitivity to dynamic responses. This stems from AV passengers' increased awareness of lateral motions when relieved from active driving tasks [21].

Table 5 compiles the maximum lateral acceleration A_{y_max} values along the entire travel distance S_{dri} shown in Figures 7–8, evaluating comfort levels for each parameter against AVs system requirements and comfort thresholds (referencing Tables 1 and 3). The data demonstrate that increasing design speed V_{de} elevates all response parameters under identical radius (R) conditions.

Analysis reveals a distinct speed-radius coupling effect: under low-speed (40–60 km/h) small-radius (R ≤ 200 m) conditions, A_{y_max} reaches 0.2–0.4 g (1.96–3.92 m/s^2), degrading comfort to levels 2–3 (moderately uncomfortable to moderately uncomfortable), with discomfort extending into adjacent transition curve segments. Conversely, at higher speeds (70–100 km/h) with typical minimum radii, A_{y_max} fluctuations diminish significantly, improving comfort to levels 1–2 (comfortable to moderately comfortable). Comparative analysis indicates that while the lateral friction coefficients (0.10–0.17) specified in the current Technical Standard of Highway Engineering ensure basic safety for conventional vehicles, AVs operating at absolute minimum radii consistently exceed $\mu_{max} = 0.17$, reaching above 0.20 at lower speeds, demonstrating that existing circular curve standards fail to meet AVs comfort requirements.

These results confirm that while AVs share comparable safety boundaries with conventional vehicles on small-radius circular curves, their comfort requirements are substantially more stringent. To prevent significant occupant discomfort, AVs should prioritize curve segments with radii exceeding the typical minimum values, a finding with critical implications for intelligent infrastructure upgrades and AVs path-planning algorithm optimization.

To assess the generalizability of our simulation results, we performed a comparative analysis with the simulation-based findings from Wang *et al.* [23]. Their numerical study demonstrated that small-radius curves (R = 200–300 m) at low operating speeds (V_{de} = 50–70 km/h) resulted in "moderately uncomfortable" ride quality, which aligns closely with our computational predictions.

Both simulation studies consistently indicate that low-speed operations on tight curves (R ≤ 200 m, $V_{de} \leq 60$ km/h) substantially degrade ride comfort. Conversely, appropriate speed-radius combinations (e.g., V_{de} = 70–100 km/h with R ≥ 200 m) effectively mitigate adverse dynamic responses. The agreement between our simulation outcomes and Wang *et al.*'s modeling results validates the capability of our co-simulation platform to reliably capture AVs comfort dynamics under such conditions. This cross-model validation strengthens the credibility of our findings, particularly in quantifying key parameters such as the critical adhesion coefficient (μ = 0.15–0.22) and lateral acceleration thresholds for small-radius curves.

Table 5. The maximum value of AVs motion/dynamic response parameters in the basic curve scene and its adaptation degree.

V_{de} (km/h)	R (m)	μ_{max}	[a]T	A_{y_max}	T	T
	60	0.21	[b]Y	2.3	Y	Y
40	80	0.15	Y	1.6	Y	Y
	100	0.12	Y	1.3	Y	Y
	100	0.20	Y	2.3	Y	Y
50	125	0.15	Y	1.6	Y	Y
	150	0.13	Y	1.3	Y	Y
	125	0.22	Y	2.4	Y	Y
	150	0.17	Y	1.9	Y	[c]H
60	175	0.15	Y	1.8	Y	Y
	200	0.13	Y	1.4	Y	H
	200	0.18	Y	1.9	Y	Y
	225	0.16	Y	1.7	Y	Y
70	250	0.14	Y	1.5	Y	H
	275	0.13	Y	1.4	Y	H
	300	0.11	Y	1.3	Y	H
	250	0.18	Y	2.0	Y	H
	275	0.16	Y	1.9	Y	H
	300	0.15	Y	1.7	Y	H
80	325	0.14	Y	1.5	Y	H
	350	0.13	Y	1.4	Y	H
	375	0.12	Y	1.3	Y	H
	400	0.11	Y	1.2	Y	H
	325	0.17	Y	2.0	Y	H
	350	0.16	Y	1.9	Y	H
	375	0.15	Y	1.7	Y	H
	400	0.14	Y	1.6	Y	H
90	425	0.13	Y	1.5	Y	H
	450	0.12	Y	1.4	Y	H
	475	0.12	Y	1.3	Y	H
	500	0.11	Y	1.2	Y	H
	525	0.10	Y	1.2	Y	H
	550	0.09	Y	1.1	Y	H
	400	0.18	Y	2.0	Y	H
	425	0.17	Y	1.9	Y	H
	450	0.16	Y	1.8	Y	H
	475	0.15	Y	1.7	Y	H
	500	0.14	Y	1.6	Y	H
	525	0.13	Y	1.5	Y	H
100	550	0.12	Y	1.4	Y	H
	575	0.12	Y	1.3	Y	H
	600	0.12	Y	1.2	Y	H
	625	0.11	Y	1.2	Y	H
	650	0.10	Y	1.2	Y	H
	675	0.10	Y	1.1	Y	H
	700	0.09	Y	1.1	Y	H

[a]T denotes tangent segments, [b]Y represents circular curves, and [c]H indicates transition (spiral) curves in the road alignment configuration.

4.3. Limitations and boundary conditions

The simulation results presented in Sections 4.1–4.2 were obtained under ideal operating conditions. The following limitations should be noted for practical applications:

First, the dry road friction coefficient (μ = 0.9) used in the simulations does not account for varying weather conditions. Existing research indicates that wet road surfaces typically have friction coefficients of approximately 0.5–0.7, while icy/snowy conditions may drop below 0.3, which would significantly impact the vehicle's critical friction margin $\Delta\mu$ (Equation 6). Additionally, the 8% maximum superelevation design may prove insufficient to compensate for lateral forces under low-friction conditions.

Second, real-world traffic interactions affect control performance. When AVs need to avoid other vehicles on curves, their trajectories will deviate from ideal paths, resulting in increased lateral acceleration fluctuations. Furthermore, sensor performance degradation in adverse weather conditions presents challenges—for instance, rain and fog may reduce LiDAR detection accuracy.

While these limitations exist, the findings of this study remain valuable as reference. Future research should focus on: AV performance validation under varying friction conditions ($\mu \in [0.3, 0.7]$), multi-vehicle cooperative simulation testing, and sensor fusion algorithm optimization for complex environments.

5. Conclusion

This study investigates the intrinsic mechanisms by which small-radius circular curves impact on the adaptability of AVs, using a high-fidelity co-simulation platform. The analysis yields three principal findings:

First, circular curve radius is a critical constraint for both AVs safety and comfort. Under low-speed conditions (40–60 km/h), segments with absolute minimum radius generate lateral acceleration and critical adhesion coefficients that approach safety thresholds. While these conditions do not cause skid instability, they significantly degrade occupant comfort, necessitating active speed reduction or path planning avoidance strategies.

Second, increased speed (70–100 km/h) and larger radii effectively suppress dynamic response fluctuations, reducing peak lateral acceleration to 1.2–2.0 m/s² and improving comfort to levels 1–2. This validates the stabilizing effect of appropriately matched speed-radius configurations.

Third, conventional road design standards specify lateral friction coefficients (0.10–0.17) that meet basic safety requirements but fall short in terms of AVs' comfort. At absolute minimum radii, AVs frequently exceed critical adhesion coefficients (0.15–0.22), highlighting the inadequacy of current standards for autonomous systems and understanding the need for targeted optimization of alignment parameters.

While the research findings were obtained under idealized dry pavement conditions (μ = 0.9) and single-vehicle scenarios, they provide quantitative foundations for AV-dedicated road design. To further enhance the engineering applicability of these findings, future research should prioritize the following areas:

(1) Establishing a validation framework for low-friction conditions ($\mu < 0.5$) including rain, snow, and icy surfaces.

(2) Developing simulation frameworks incorporating dynamic interactions in mixed traffic flows.

(3) Investigating V2I-based real-time curve parameter transmission and predictive control technologies.

(4) Formulating evaluation methodologies for AV dynamics under the coupled effects of vertical grades and combined alignments.

These extended studies will advance the precise definition of Operational Design Domains (ODD) for autonomous driving systems, while providing more comprehensive technical support for intelligent infrastructure adaptation and AV control algorithm optimization.

Acknowledgments

The authors would like to thank National Natural Science Foundation of China (Grant No. 52178403). Their support is sincerely appreciated.

Authors' contribution

Zhiqing Zhang: writing—review & editing supervision, funding acquisition. Xiaozheng Yu: writing—original draft, software, methodology, conceptualization. Leipeng Zhu: project administration, formal analysis. Min Wang: writing—review & editing supervision. All authors have read and agreed to the published version of the manuscript.

Conflicts of interests

The authors declare no conflict of interest.

References

[1] Gao S, Liu P. 2018 Uber automated vehicle accident analysis: from an HFACS perspective (In Chinese). *Chin. J. Ergon.* 2022, 28(1):30–36

[2] Wang S, Yu B, Ma Y, Liu J, Zhou W. Impacts of different driving automation levels on highway geometric design from the perspective of trucks. *Adv. Transp.* 2021, 1:5541878.

[3] Yu B, Wang S, Ma Y. Review of driving adaptability of intelligent vehicles to as-built roadway infrastructures (In Chinese). *Chin. J. Highw. Transp.* 2022, 35(10):205–225.

[4] Xu X, Wang X, Wu X, Hassanin O, Chai C. Calibration and evaluation of the responsibility-sensitive safety model of autonomous car-following maneuvers using naturalistic driving study data. *Transp. Res. Part C Emerg. Technol*. 2021, 123:102988.

[5] Jing S, Hui F, Zhao X, Rios-Torres J, Khattak AJ. Integrated longitudinal and lateral hierarchical control of cooperative merging of connected and automated vehicles at on-ramps. *IEEE Trans. Intell. Transp. Syst*. 2022, 23(12):24248–24262.

[6] Zhu B, Jiang Y, Zhao J, He R, Bian N, *et al.* Typical-driving-style-oriented personalized adaptive cruise control design based on human driving data. *Transp. Res. Part C Emerg. Technol*. 2019, 100:274–288.

[7] Ye X, Wang X, Liu S, Tarko AP. Feasibility study of highway alignment design controls for autonomous vehicles. *Accid. Anal. Prev.* 2021, 159:106252.

[8] Lengyel H, Tettamanti T, Szalay Z. Conflicts of automated driving with conventional traffic infrastructure. *IEEE Access* 2020, 8:163280–163297.

[9] Chang I, Lee J, Ahn S. Evaluation of level 2 automated driving safety on curved sections. *KSCE* J. *Civ. Eng*. 2024, 28(9):4023–4031.

[10] Wang S, Yu B, Ma Y, Liu J, Zhou W. Impacts of different driving automation levels on highway geometric design from the perspective of trucks. *J. Adv. Transpor*. 2021, 2021(1):5541878.
[11] Alfredo G, Camacho-Torregrosa FJ, Baez P. Examining the effect of road horizontal alignment on the speed of semi-automated vehicles. *Accid. Anal. Prev.* 2020, 146:10573.
[12] Xia H. Research on trajectory planning and coupled motion control of autonomous vehicle in curve driving (In Chinese). Doctoral Thesis, SCUT, 2020.
[13] Zhou W. Research on safety evaluation of road alignment design for autonomous driving (In Chinese). Master's Thesis, SEU, 2022.
[14] Yu H, Zhao X, Nan C, Yang L, Li J. Accident-prone section prediction models for intelligent vehicles based on road alignment (In Chinese). *China J. Highw. Transp.* 2021, 34(3):183–192.
[15] Wang X, Coulibaly NM, Zeng Q. Influence of highway space alignment continuous degradation in 3-dimensional space on autonomous vehicle trajectory deviation based on PreScan simulation. *Digit. Transp. Saf.* 2023, 2(2):77–88.
[16] China Communications First Highway Survey and Design Institute. *Design Specification For Highway Alignment JTG D20-2017* (In Chinese). Beijing: China Communications Press, 2017.
[17] Yu M, Qian Y, Huang H, Wang Z. Lateral and longitudinal coupling control of autonomous vehicle based on PID + LQR algorithm under continuous conditions (In Chinese). *Sci. Technol. Eng.* 2022, 22(30):13490–13496.
[18] Ma Y, Easa S, Cheng J, Yu B. Automatic framework for detecting obstacles restricting 3D highway sight distance using MLS eata. *J. Comput. Civ. Eng.* 2021, 35(4):04021008.
[19] Li S. Lateral acceleration estimation based on wheel SpeedSignal & curving braking control algorithm research (In Chinese). Master's Thesis, JLU, 2008.
[20] Yasmany GR, Diego AC. Passengers' comfort in horizontal curves on mountain roads: a field study using lateral accelerations. *Rev. Fac. Ing.* 2021, 98:94–103.
[21] Jin X, Kui Y, Yiming S, Gong L. An experimental study on lateral acceleration of cars in different environments in Sichuan, southwest China. *Discrete Dyn. Nat. Soc.* 2015, 2015(1):494130.
[22] China First Highway Survey and Design Institute. *Technical standard of highway engineering JTG B01-2014* (In Chinese). Beijing: People's Transportation Press, 2014.
[23] Wang S, Lai Y, Qiu X, Ma Y, Easa SM, *et al*. Implications of as-built highway horizontal curves on vehicle dynamics/kinematics characteristics under adaptive cruise control. *IET Intel. Transport Syst.* 2025, 19(1):e12604.